Dissecting the role of interprotomer cooperativity in the activation of oligomeric high-temperature requirement A2 protein

Yuki Toyama[a,b,c,1], Robert W. Harkness[a,b,c], and Lewis E. Kay[a,b,c,d,1]

[a]Department of Molecular Genetics, University of Toronto, Toronto, ON M5S 1A8, Canada; [b]Department of Biochemistry, University of Toronto, Toronto, ON M5S 1A8, Canada; [c]Department of Chemistry, University of Toronto, Toronto, ON M5S 3H6, Canada; and [d]Program in Molecular Medicine, Hospital for Sick Children Research Institute, Toronto, ON M5G 0A4, Canada

Edited by Adriaan Bax, NIH, Bethesda, MD, and approved July 23, 2021 (received for review June 17, 2021)

The human high-temperature requirement A2 (HtrA2) mitochondrial protease is critical for cellular proteostasis, with mutations in this enzyme closely associated with the onset of neurodegenerative disorders. HtrA2 forms a homotrimeric structure, with each subunit composed of protease and PDZ (PSD-95, DLG, ZO-1) domains. Although we had previously shown that successive ligand binding occurs with increasing affinity, and it has been suggested that allostery plays a role in regulating catalysis, the molecular details of how this occurs have not been established. Here, we use cysteine-based chemistry to generate subunits in different conformational states along with a protomer mixing strategy, biochemical assays, and methyl-transverse relaxation optimized spectroscopy–based NMR studies to understand the role of interprotomer allostery in regulating HtrA2 function. We show that substrate binding to a PDZ domain of one protomer increases millisecond-to-microsecond timescale dynamics in neighboring subunits that prime them for binding substrate molecules. Only when all three PDZ-binding sites are substrate bound can the enzyme transition into an active conformation that involves significant structural rearrangements of the protease domains. Our results thus explain why when one (or more) of the protomers is fixed in a ligand-binding–incompetent conformation or contains the inactivating S276C mutation that is causative for a neurodegenerative phenotype in mouse models of Parkinson's disease, transition to an active state cannot be formed. In this manner, wild-type HtrA2 is only active when substrate concentrations are high and therefore toxic and unregulated proteolysis of nonsubstrate proteins can be suppressed.

human high-temperature requirement A2 | ligand-binding thermodynamics | cooperativity | protein allostery | methyl-transverse relaxation optimized NMR spectroscopy

The accumulation of unfolded and/or misfolded proteins leads to cell damage and malfunction, and an elaborate protein quality control machinery has evolved to mitigate these stresses. The widely conserved high-temperature requirement A (HtrA) proteins play central roles in protein quality control where, in response to aberrantly folded client proteins, they can act as either proteases (protein recycling) or chaperones (protein refolding) in an adenosine 5′-triphosphate–independent manner (1, 2). Human HtrA2, also known as the Omi protease, is a mitochondrial HtrA protease localized primarily to the mitochondrial intermembrane space (3–5). HtrA2 has been well characterized as a key regulator of apoptotic signaling (5–12), and it also functions as a stress-protective protease in mitochondria. For example, HtrA2 plays a prominent neuroprotective role by regulating the levels of unfolded proteins in mitochondria, which, if left unchecked, contribute to the onset of neurodegenerative disorders (13–17). This important role for HtrA2 is supported by the observation that missense mutations in the *HTRA2* gene were found in patients with Parkinson's disease and essential tremor (18, 19). Further evidence for the essential relationship between HtrA2 function and neuroprotection was established by the demonstration that an inactivating HtrA2 point mutation is causative for the neurodegenerative phenotype in the *mnd2* (motor neuron degeneration 2) mouse, which is considered to be an animal model for Parkinson's disease (20).

HtrA2 protomers contain one copy each of a protease and a PDZ (PSD-95, DLG, ZO-1) domain. The crystal structure of HtrA2 shows that three protomers form a pyramid-shaped homotrimer in which the interprotomer interactions are mediated by the protease domains (pink) (21) (Fig. 1 *A*, *Inset*). The crystal structure is thought to represent an inactive conformation whereby the catalytic triad within the protease domain, formed by H198, D228, and S306, is covered by the PDZ domain (light blue) to form a tightly packed closed structure (2, 21). The PDZ domain harbors a canonical ligand-binding pocket, where a short hydrophobic activator peptide or the C terminus of substrate proteins can bind, leading to an open conformation, and ultimately, catalysis when substrate peptides or regions of substrate proteins bind to the protease domain (21–25). Since structures of neither an open conformation nor a substrate-bound state are available, details of the HtrA2 activation mechanism have long remained elusive. Using solution NMR spectroscopy focusing on side-chain methyl groups, we have recently shown that HtrA2 exchanges between a canonical trimer and a previously unobserved hexamer in solution with the activator peptide preferentially binding to the trimeric form of the enzyme. The

Significance

The HtrA2 enzyme removes toxic proteins in mitochondria, ensuring proper cellular function. HtrA2 malfunction is associated with neurodegenerative disorders such as Parkinson's disease and essential tremor. HtrA2 is composed of three copies of a protein chain, and the ways in which these chains communicate to form a functional enzyme are not well understood. Here, we have used NMR spectroscopy in concert with a strategy for producing trimers containing different types of chains to elucidate the mechanisms by which the HtrA2 enzyme is regulated. Our data lead to a model explaining how HtrA2 suppresses proteolysis of nonsubstrate proteins and, furthermore, how a single point mutation in HtrA2 that leads to neurodegeneration in mice gives rise to an inactive enzyme.

Author contributions: Y.T., R.W.H., and L.E.K. designed research; Y.T., R.W.H., and L.E.K. performed research; Y.T., R.W.H., and L.E.K. analyzed data; and Y.T. and L.E.K. wrote the paper.

The authors declare no competing interest.

This article is a PNAS Direct Submission.

[1]To whom correspondence may be addressed. Email: kay@pound.med.utoronto.ca or yuki.toyama@utoronto.ca.

This article contains supporting information online at https://www.pnas.org/lookup/suppl/doi:10.1073/pnas.2111257118/-/DCSupplemental.

Published August 26, 2021.

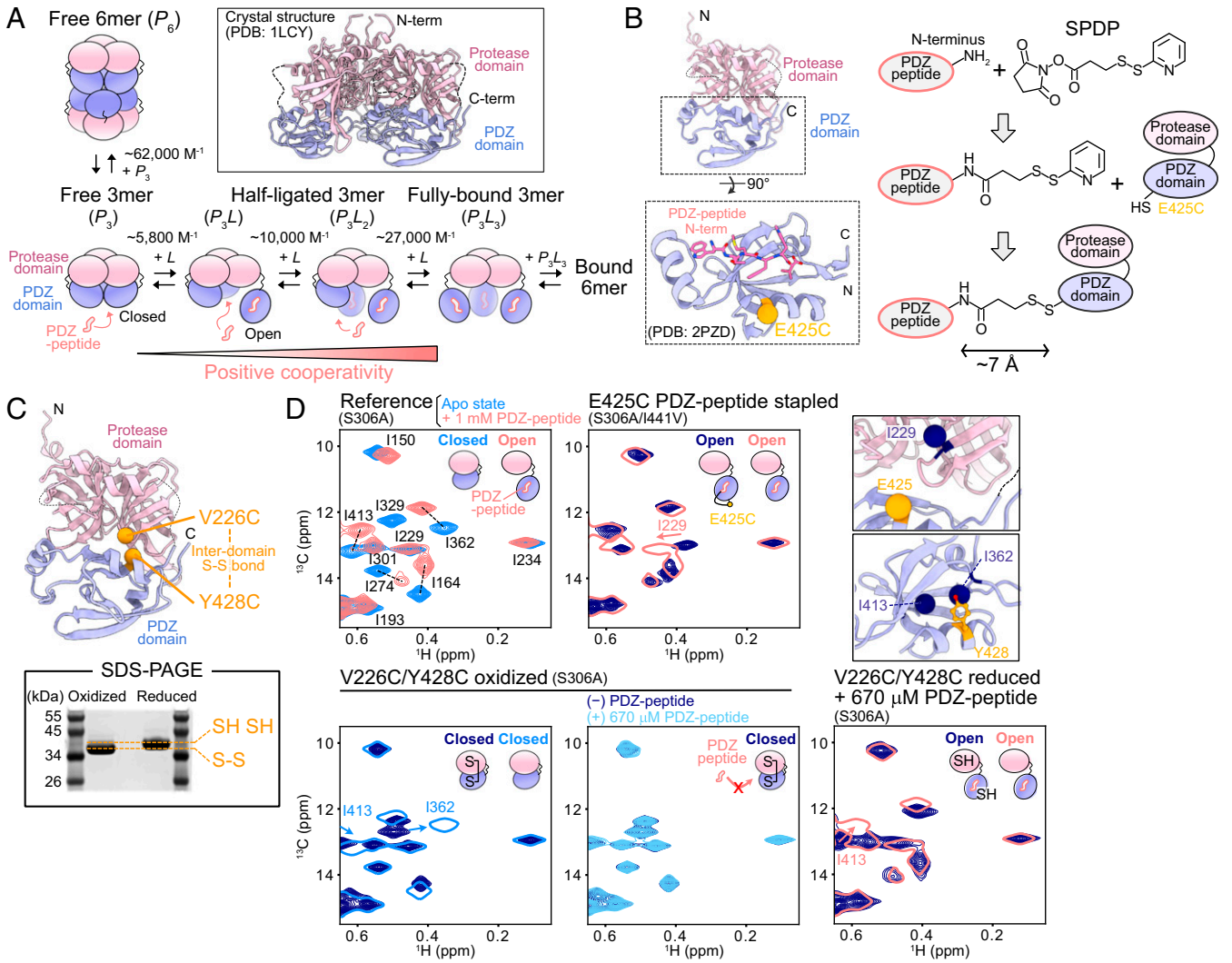

Fig. 1. Controlling domain opening via Cys-based chemistry. (*A*) The oligomerization and PDZ-peptide binding mechanism of HtrA2, as established in our previous study (26). (*Inset*) Crystal structure of trimeric HtrA2 (PDB ID: 1LCY). The protease (residues 134 to 345) and PDZ (residues 359 to 458) domains are colored pink and light blue, respectively. Electron density for residues 282 to 290 (β8-β9 linker) and 344 to 358 (interdomain linker) is not observed; these regions are shown with dotted lines. (*B*) The crystal structure of the isolated PDZ domain of HtrA2 in complex with peptide (WTMFWV; PDB ID: 2PZD). The peptide is shown as a pink stick model with the E425 Cβ carbon displayed as an orange sphere. Chemical structures of the components involved in the Cys modification approach to control the peptide-bound state of the PDZ domain are shown on *Right*. (*C*, *Top*) The Cβ carbons of V226 and Y428 are displayed on an HtrA2 protomer (PDB ID: 1LCY). (*Bottom*) SDS-PAGE analysis of V226C/Y428C/S306A HtrA2 under oxidizing and reducing conditions. (*D*, *Left Top*) ^{13}C-^{1}H HMQC spectra of U-^{2}H, *proR* ILVM S306A HtrA2 in the absence (blue) and presence (pink) of 1 mM PDZ-peptide. (*Center Top*) ^{13}C-^{1}H HMQC spectrum of U-^{2}H, *proR* ILVM S306A/I441V/E425C PDZ-peptide–stapled HtrA2 (navy). The spectrum of U-^{2}H, ILVM S306A/I441V HtrA2 in the presence of 1 mM PDZ-peptide is shown using pink single contours. (*Left Bottom*) ^{13}C-^{1}H HMQC spectrum of U-^{2}H, *proR* ILVM V226C/Y428C/S306A HtrA2 under oxidizing conditions. The spectrum of U-^{2}H, *proR* ILVM S306A HtrA2 is shown with single blue contours. (*Center Bottom*) Superposition of ^{13}C-^{1}H HMQC spectra of U-^{2}H, *proR* ILVM V226C/Y428C/S306A HtrA2 in the absence (navy) and presence of 670 μM PDZ-peptide (cyan) under oxidizing conditions. (*Right Bottom*) ^{13}C-^{1}H HMQC spectrum of U-^{2}H, *proR* ILVM V226C/Y428C/S306A HtrA2, fully reduced and in the presence of 670 μM PDZ-peptide (navy). The spectrum of U-^{2}H, *proR* ILVM S306A HtrA2 in the presence of 1 mM PDZ-peptide is shown with pink single contours. Schematics of the protomeric structures that form the HtrA2 trimers studied by NMR are shown in the upper right hand corner of each spectrum. (*Right Top*) The methyl groups with significant chemical shift differences in the comparative spectra shown (i.e., between Cys and Cys-less molecules) (navy spheres) are in the immediate vicinity of the mutated residues (Cβ carbon of E425 shown as an orange sphere and side-chain atoms of Y428 shown as orange sticks) (PDB ID: 1LCY). Methyl group assignments of the S-S–locked and PDZ-peptide–stapled samples were obtained by inspection of spectra of the closed and open structures, respectively, as there were only minor chemical shift differences. All NMR data were recorded at 23.5 Tesla and 40 °C.

binding of the activator peptide to the PDZ domain occurs with positive cooperativity, subsequently leading to an open PDZ conformation that facilitates substrate engagement as summarized in Fig. 1*A* (26). Although these NMR results present a picture of how different oligomeric forms of HtrA2 regulate activator peptide binding and hint of the importance of allostery in controlling activity, a number of critical questions remain. First, what constitutes a catalytically active state at the level of individual protomers? That is, does binding of activator peptide to a given subunit lead to activity in a manner independent of the binding status of neighboring protomers, or do all protomers require activation before catalysis can occur, and, if so, how is this controlled structurally? Second, what is the structural mechanism underlying the loss of function of various HtrA2 disease mutants? One such example is provided by an S276C mutant that was identified in *mnd2* mutant mice (20). Although the high-resolution crystal structure of the

closed, catalytically inactive mutant was solved and an altered bound-water network around residue 276 was observed (27), the overall structure of this mutant was similar to the corresponding structure of the protein without the S276C mutation (RMSD 0.244 Å). Therefore, the detailed structural basis for why the S276C mutant is inactive remains unknown.

A critical determinant of function and malfunction in the HtrA2 system is likely to be interprotomer allostery within the trimeric enzyme architecture, controlling the structural changes that accompany the transition from the closed, inactive conformation to the catalytically active, open form of the molecule. Previous studies have provided qualitative evidence of the importance of interprotomer allostery for activation of HtrA2, since an engineered monomeric mutant of HtrA2 was shown to be nonfunctional both in vitro and in cells (21, 28, 29). Our previous NMR study, establishing positive cooperativity for the binding of activator peptide, also pointed to intersubunit communication (26) but did not provide insight into its origin, suggesting the need for a more detailed investigation of allosteric signaling pathways between HtrA2 protomers. NMR is a particularly powerful technique to analyze such interprotomer interactions, as it can be used to monitor the microscopic chemical environment of individual nuclear spins from each protomer and, hence, to provide a detailed, and sometimes atomistic, picture of the structural consequences of perturbations that occur in neighboring protomers (30). This is in contrast to other biophysical techniques in which insight about interprotomer allostery is usually less direct, obtained by analyzing macroscopic observables and fitting them to models that take into account cooperativity (31). Moreover, NMR informs on the structural dynamics of proteins, which play a central role in interprotomer allosteric communication (32–34). In practical applications involving homo-oligomeric proteins such as HtrA2, however, detailed structural analyses of interprotomer allostery have remained challenging due to the difficulty in isolating asymmetric conformers (i.e., partially ligated states) coupled with the fact that individual protomers usually do not give rise to unique chemical shifts that can be independently resolved and analyzed so as to establish structural differences between subunits. For these reasons, NMR analyses of interprotomer allostery in homo-oligomeric proteins have generally been limited to systems with strong negative cooperativity (35, 36).

Here, to investigate how interprotomer allosteric communication leads to a modulation of HtrA2 function, we have used methyl-transverse relaxation optimized spectroscopy (methyl-TROSY) NMR in combination with a protomer mixing strategy in which one of the protomers in the trimer is selectively observed. To overcome the difficulties in analyzing asymmetric states, discussed above, we have used cysteine (Cys)-based chemistry to stably control domain opening of and activator or substrate peptide binding to each protomer. We demonstrate that the microsecond-to-millisecond (μs–ms) timescale dynamics of the observed protomer change in response to the open/closed status of PDZ domains on neighboring subunits, underlying the positive cooperativity of activator peptide binding. We also establish that the formation of an active conformation of the protease domain is tightly regulated through interprotomer interactions so that the catalytically active conformation is solely formed when all three PDZ domains in the trimer are occupied by activator peptides. Finally, we show that the loss of function in the S276C disease mutant results from an inability to form the catalytically active conformation, suggesting that subtle disruptions of interprotomer allosteric networks are responsible for HtrA2 malfunction and the onset of associated neurological disorders.

Results

Using Cys-Based Chemistry to Control the Peptide-Bound State of Each Protomer. Fig. 1*A* shows a schematic model for the sequential binding of an activator peptide to HtrA2 and the concomitant conformational changes involving PDZ domain opening that was proposed in our previous study (26). In the absence of the activator peptide, HtrA2 is in equilibrium between a hexamer (P_6) and a canonical trimer (P_3), with the activator peptide interacting much more tightly with the trimeric state so that binding to the hexamer can be neglected. The activator peptide binds to P_3, P_3L, and P_3L_2 sequentially to form the fully bound P_3L_3 state in which L denotes the activator peptide that binds to the PDZ domain. In our former NMR titration analyses, the binding isotherms could be explained by a model in which domain opening occurs through the binding of the activator peptide to each protomer individually, leading to the formation of asymmetric structures for P_3L (two closed protomers and one open protomer) and P_3L_2 (one closed protomer and two open protomers). We note that the fully bound trimer, P_3L_3, can further dimerize to form a fully bound hexameric state, P_6L_6; however, in what follows, our emphasis is on studies of interprotomer allostery within a trimeric unit (*SI Appendix*).

As a first step, we sought to focus on the partially ligated trimers, P_3L and P_3L_2, as these inform on structural changes and interprotomer allostery along the pathway to the fully activated state of HtrA2. A major challenge in these analyses is that the populations of the asymmetric P_3L or P_3L_2 states shift with increasing activator peptide concentration, reaching maximal values of only ∼30% (as a fraction of protomers in each state), hampering a detailed NMR analysis (26). This is a direct result of the relatively modest increase in successive peptide-binding affinities to the PDZ domains (K_2∼$2K_1$, K_3∼$3K_2$, Fig. 1). Also, these asymmetric species are difficult to isolate, and NMR spectra recorded at a given ligand concentration will, therefore, potentially contain contributions from all of the different ligated states, both symmetric and asymmetric, complicating a focus on the asymmetric species of interest. To overcome this problem, we sought to establish a strategy to stably control the peptide-bound state of each protomer of HtrA2 by utilizing Cys-based chemistry. HtrA2 does not have any intrinsic Cys residues in its amino acid sequence. Thus, by introducing Cys mutations, it is possible to either covalently link activator peptides to their binding sites in the PDZ domains to ensure PDZ domain opening or to introduce an intraprotomer disulfide bond to fix the PDZ domains in their closed positions so as to prohibit binding of the activator peptide. By using these covalently modified subunits and a protomer mixing strategy (see *Titrations of Asymmetric HtrA2 Trimers Establish Positive PDZ-Peptide–Binding Cooperativity* for details), it becomes possible to carry out detailed structural studies of stably formed asymmetric particles.

In order to mimic the native activator peptide-bound/open conformation, we introduced a single Cys mutation to the PDZ domain and covalently attached the activator peptide via an intermolecular cross-link (referred to in what follows as "peptide stapled"). To this end, a short-chain cross-linker was used, *N*-succinimidyl 3-(2-pyridyldithio) propionate (SPDP), which cross-links a free amine group to a sulfhydryl group at the introduced Cys side chain (37) via a two-step procedure (Fig. 1*B*). Residue 425 (E425) was chosen as the Cys-modification site on the PDZ domain, guided by the crystal structure of the isolated PDZ domain in complex with a short hydrophobic peptide (22). As an activator peptide, we used an octapeptide DD-PDZopt (DDGQYYFV), subsequently referred to as PDZ-peptide, which has high water solubility and binds to HtrA2 with association constants ranging from 5,800 M^{-1} (binding to P_3) to 27,000 M^{-1} (binding to P_3L_2) (Fig. 1*A*) (26).

In order to ensure that a given protomer assumes a tightly packed closed conformation, hence preventing the binding of PDZ-peptide to it, we designed a double Cys mutant to introduce an intraprotomer/interdomain disulfide bond which affixes the PDZ domain to the protease domain (hereafter referred as an "S-S lock") (38–41). By carefully inspecting the crystal structure of HtrA2 in the closed conformation (Protein Data Bank identification [PDB ID]: 1LCY) (21), we identified a pair of residues, V226 and Y428, whose side chains are directed toward each other with an interdomain Cβ-Cβ distance (5.3 Å) that is the shortest among all possible pairs. We introduced a double Cys mutation

(V226C/Y428C) and confirmed the formation of the expected intraprotomer disulfide bond based on a redox-dependent HtrA2 band shift in sodium dodecyl sulfate–polyacrylamide gel electrophoresis (SDS-PAGE) gels (Fig. 1*C*).

We then tested whether these PDZ-peptide–stapled and S-S–locked versions of HtrA2 closely mimic the native open and closed structures, respectively, by measuring their NMR spectra. We prepared samples of these constructs with $^{13}CH_3$ labeling at Ileδ1, Leuδ1 (*proR*), Valγ1 (*proR*), and Metε positions in an otherwise deuterated background (referred to as U-^{2}H, *proR* ILVM-$^{13}CH_3$ labeling in what follows) (42–44) and measured ^{13}C-^{1}H heteronuclear multiple-quantum coherence (HMQC) spectra in which a methyl-TROSY effect leads to improvements in spectral sensitivity and resolution (45). In all of the following NMR analyses, two background mutations were added (unless indicated otherwise), including S306A, in which the catalytic Ser is replaced by Ala to suppress self-cleavage at high protein concentrations, and I441V, which suppresses hexamerization of HtrA2 in the apo state (26). As shown in Fig. 1 *D*, *Top Left*, significant chemical shift changes of Ile methyl signals were observed upon the addition of 1 mM PDZ-peptide to the native protein (i.e., no Cys modifications; blue and pink contours) (Fig. 1*D* and *SI Appendix*, Fig. S1*A*). These Ile methyl signals were used, therefore, as a fingerprint to evaluate the structure of the Cys-modified mutant proteins. As ILVM-methyl groups are well distributed throughout HtrA2, the structural dynamics of both PDZ and protease domains can be readily probed by recording ^{13}C-^{1}H HMQC datasets. We first measured the HMQC spectrum of U-^{2}H, *proR* ILVM-$^{13}CH_3$ E425C PDZ-peptide–stapled HtrA2 (in the absence of added PDZ-peptide) and compared it with that of unmodified HtrA2 recorded in the presence of excess PDZ-peptide (1 mM). The Ile methyl chemical shifts of E425C PDZ-peptide–stapled HtrA2 were in good agreement with those of the PDZ-peptide–bound state of the unmodified protein (Fig. 1 *D*, *Top Middle*, compare navy contours with single pink contour, *SI Appendix*, Fig. S1*B*), showing that the E425C PDZ-peptide–stapled conformation closely mimics that of the native PDZ-peptide–bound state. We also measured the HMQC spectrum of U-^{2}H, *proR* ILVM-$^{13}CH_3$ V226C/Y428C S-S–locked HtrA2 (note that the I441V mutation was not introduced here). The Ile methyl chemical shifts were mostly consistent with those of the apo/closed state of the native protein (Fig. 1 *D*, *Bottom Left*, blue single contour), and the spectrum did not change upon the addition of excess PDZ-peptide (670 μM), showing that the S-S–locked protein forms a closed conformation that is not accessible to peptide (Fig. 1 *D*, *Bottom Middle*). Importantly, the inhibition of PDZ-peptide binding in the S-S–locked state is reversible, as the spectrum recorded after the reduction of the interdomain S-S bond by the addition of 5 mM dithiothreitol (DTT) to the aforementioned sample is consistent with a PDZ-peptide–bound/open HtrA2 conformation (Fig. 1 *D*, *Bottom Right*, compare navy and pink contours). We note that some of the Ile residues showed chemical shift changes in spectra that were compared, such as I166 and I229 in E425C PDZ-stapled HtrA2 (Fig. 1 *D*, *Top Right* and *SI Appendix*, Fig. S1*B*) and I333, I362, I373, and I413 in V226C/Y428C S-S–locked HtrA2 (Fig. 1 *D*, *Bottom Left* and *SI Appendix*, Fig. S1*C*). These Ile residues are proximal to the mutational sites (Fig. 1 *D*, *Top Right* and *SI Appendix*, Fig. S1*D*) so that the observed shift differences are likely due to structural perturbations resulting from mutations and/or slight changes in the orientation of the PDZ-peptide between open-stapled and open-bound (but not cross-linked) forms.

Titrations of Asymmetric HtrA2 Trimers Establish Positive PDZ-Peptide–Binding Cooperativity. Having developed a Cys-based protocol to control PDZ-peptide binding to, and hence the open/closed status of, individual protomers in HtrA2, we next sought to investigate aspects of interprotomer allosteric communication, including the verification of the positive PDZ-peptide–binding cooperativity that had been inferred from previous fits of titration data (26). We, therefore, adopted a protomer mixing strategy to produce stably formed asymmetric HtrA2 trimers for NMR analyses in which some of the subunits were either in closed/S-S–locked or open/PDZ-stapled states (41, 46, 47).

The mixing protocol is summarized in Fig. 2*A*. Native HtrA2 was prepared with U-^{2}H, *proR* ILV-$^{13}CH_3$ labeling (NMR visible, Fig. 2*A*, green circles) along with a second preparation composed of V226C/Y428C or E425C HtrA2 with uniform ^{2}H labeling or $^{13}CH_3$ labeling of only the Met methyl groups (NMR invisible in the Ile, Leu, and Val spectral region; Fig. 2*A*, black-filled circles). The two protein preparations were mixed in molar ratios of 10% (native):90% (Cys mutant), denatured by the addition of 6 M guanidinium chloride and refolded by rapid dilution, and subsequently, the Cys side-chain sulfhydryl groups were oxidized to form an interdomain S-S bond or reacted with SPDP-modified PDZ-peptide (Fig. 2 *A*, *Right*). During the refolding process, the protomers reassembled into trimers randomly, and the distribution of subunits within each particle gives rise to four different configurations (A–D in Fig. 2*A*) whose populations can be readily calculated. The random mixing of protomers was experimentally verified as previously described (*SI Appendix*, Fig. S2) (41), and we have established that the unfolding/refolding protocol did not perturb the structure of the trimer nor did it affect its enzymatic activity (*SI Appendix*, Fig. S3). The symmetric trimers A and D do not contribute to the NMR spectrum, as all of the protomers are either NMR invisible (configuration A) or NMR visible but at a concentration too low for detection (configuration D, $0.1^3 \times 100 = 0.1\%$ of the particles). The major contribution to the NMR spectrum is therefore from configuration B (one NMR-visible native protomer, two NMR-invisible Cys protomers; $3 \times 0.9^2 \times 0.1 \times 100 = 24.3\%$ of particles) with a smaller contribution from configuration C (two NMR-visible protomers, one NMR-invisible Cys protomer; $3 \times 0.9 \times 0.1^2 \times 100 = 2.7\%$ of particles). Thus, the 10%:90% mixing scheme used (Fig. 2*A*) provides an opportunity to focus on a native protomer in the context of two NMR-invisible neighbors that are either S-S–locked or PDZ-peptide stapled and hence observe how the closed or open states of adjacent protomers influence the structural dynamics of a neighboring protomer. In this manner, the role of interprotomer communication can be established directly.

Fig. 2*B* highlights the two types of NMR-observable samples prepared: 1) sample one was obtained by mixing 90% U-^{2}H, M-$^{13}CH_3$ V226C/Y428C S-S–locked protomers and 10% U-^{2}H, *proR* ILV-$^{13}CH_3$ native protomers to selectively observe the unbound, native protomer adjacent to closed/S-S–locked protomers (*Left*), and 2) sample two was generated by mixing 90% U-^{2}H, M-$^{13}CH_3$ E425C PDZ-peptide–stapled protomers and 10% U-^{2}H, *proR* ILV-$^{13}CH_3$ native protomers to observe the unbound protomer adjacent to open/PDZ-stapled protomers (*Right*). A comparison of HMQC spectra of these samples recorded in the absence of added PDZ-peptide (green, multiple contours) with a spectrum of the symmetric closed trimer (blue single contour), focusing on the Ile region in Fig. 2*B*, establishes that the native protomers adopt the unbound/closed conformation regardless of the status of the neighbors. Notably, small chemical shift perturbations (CSPs) were more prevalent in spectra of sample two, likely reflecting long-range interprotomer allosteric communication that is more pronounced when neighbors adopt the open/PDZ-peptide–bound conformation as discussed in *Changes in Structure and Dynamics Lead to Interprotomer Allostery*.

The asymmetric samples that have been prepared can be used to directly investigate whether the binding of the PDZ-peptide to HtrA2 occurs in a cooperative manner. Since the predominant trimer configuration in these samples contains a single binding-competent protomer that is also the only subunit of the three that is NMR active, we analyzed binding isotherms according to a simple two-state model to obtain an estimate of binding affinities.

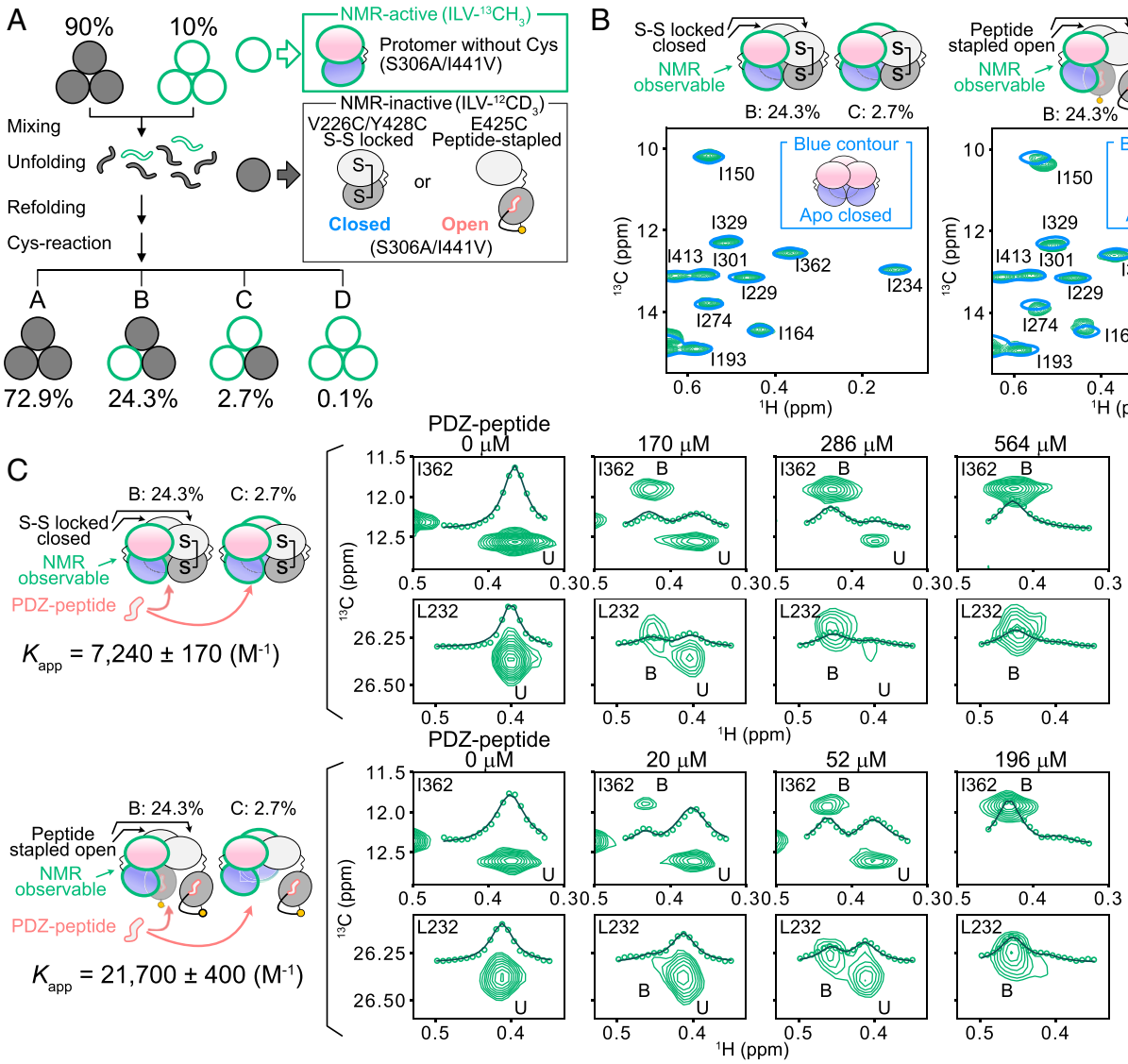

Fig. 2. Sequential PDZ-peptide binding with positive cooperativity. (*A*) Schematic highlighting the strategy for preparing mixed protomer HtrA2 samples. (*Left*) The HtrA2 trimer is shown schematically by three circles. (*Right*) NMR-visible (U-^{2}H, *proR* ILV-$^{13}CH_3$-labeled) S306A/I441V protomers are shown as green circles and NMR-(ILV)invisible (U-^{2}H, Met-$^{13}CH_3$-labeled) V226C/Y428C/S306A/I441V or E425C/S306A/I441V protomers are shown as gray-filled circles. The four different types of HtrA2 trimers obtained upon protomer mixing are shown with their expected fractional populations (particles A to D, *Bottom*). Only one out of the three possible rotationally symmetric configurations is shown for particles B and C for brevity. (*B*) ^{13}C-^{1}H HMQC spectra of asymmetric HtrA2 samples prepared by mixing 1) 90% U-^{2}H, Met-$^{13}CH_3$ V226C/Y428C/S306A/I441V S-S–locked/closed protomers and 10% U-^{2}H, *proR* ILV-$^{13}CH_3$ S306A/I441V protomers (*Left*), or 2) 90% U-^{2}H, Met-$^{13}CH_3$ S306A/I441V/E425C PDZ-peptide–stapled/open protomers and 10% U-^{2}H, *proR* ILV-$^{13}CH_3$ S306A/I441V protomers (*Right*). Schematics for particles B and C that give rise to ILV-NMR signals are shown on top of each spectrum (the population of symmetric particle D is too low for detection). The spectrum of U-^{2}H, *proR* ILVM S306A/I441V HtrA2 (symmetric) is shown with blue single contours, along with its structural schematic in *Inset*. (*C*) Selected regions of ^{13}C-^{1}H HMQC spectra as a function of added PDZ-peptide concentration using sample one (*Top*) and sample two (*Bottom*), focusing on cross-peaks from I362 and L232. Association constants obtained from two-dimensional line-shape analyses are shown on *Left*, along with the schematics of the HtrA2 molecules titrated. Experimental ^{1}H one-dimensional projections (dot) and the fitted values (line) that trace the maximum intensities in the displayed regions are shown. The signals from the unbound and bound protomers are denoted as U and B, respectively. The concentration of HtrA2 in all samples was 200 μM (subunit concentration) so that the effective concentration of NMR-active protomers for particles B and C was 16 and 3.6 μM, respectively. All NMR datasets were recorded at 14.0 Tesla and 40 °C.

Notably, PDZ-peptide binding is slow on the NMR chemical shift timescale, as separate unbound (U) and bound (B) peaks are observed (Fig. 2*C*). Some peaks were significantly broadened in the middle of the titration, especially for sample one, due to exchange-induced broadening between U and B states. Therefore, a global analysis of two-dimensional line shapes, rather than peak heights, was performed to extract apparent association constants using the program TITAN (48). Using sample one, $K_1 = 7{,}240 \pm 170$ M^{-1} was estimated for the association constant for the binding of the first ligand to HtrA2 ($P_3 + L \rightarrow P_3L$; Fig. 2 *C*, *Top*), while a similar ligand titration using sample two, reporting primarily on the binding of the third ligand ($P_3L_2 + L \rightarrow P_3L_3$), yielded $K_3 = 21{,}700 \pm 400$ M^{-1} (Fig. 2 *C*, *Bottom*). Thus, the binding affinity of the PDZ-peptide is tighter when neighboring protomers are in the open/PDZ-peptide–bound conformation. Notably, the *K* values obtained presently are in excellent agreement with affinities from an analysis of binding isotherms recorded on a symmetric HtrA2 sample and fit to a sequential association mechanism (5,800 ± 1,100 M^{-1},

10,000 ± 3,000 M^{-1}, 27,000 ± 4,000 M^{-1} for the first, second, and third binding events, respectively) (26). Interestingly, while the affinities for the PDZ-peptide are relatively low, separate peaks are, nevertheless, observed for free and bound conformations. This suggests that ligand binding is coupled to a conformational change from a closed, unligated state in which PDZ and protease domains are juxtaposed to an open conformation as described previously (26).

In summary, our data establish that native/unbound protomers adopt the closed conformation regardless of their neighbors, with the binding of the PDZ-peptide triggering domain opening. Furthermore, PDZ domain opening occurs in a sequential manner with positive cooperativity so that successive binding steps are of higher affinity as the number of protomers in the open conformation increases.

Changes in Structure and Dynamics Lead to Interprotomer Allostery. The titration experiments performed on the asymmetric samples described above establish a higher PDZ-peptide–binding affinity when neighboring subunits are open/PDZ-peptide bound as opposed to closed ($K_3 > K_1$). Yet, in both cases, an incoming PDZ-peptide cannot readily access the binding cleft on the receptor protomer since it is localized to the protease-PDZ domain interface and hence sequestered (21, 22, 26) (Fig. 1*B*). It is of interest, therefore, to establish why there is a difference in binding affinity for these two types of asymmetric samples and to ascertain whether some allosteric mechanism is at play. Some insight is obtained through a close examination of the differences in spectra recorded of a symmetric native sample (Fig. 3*A* and *SI Appendix*, Fig. S4*A*, navy) and an asymmetric sample prepared by mixing 90% U-^{2}H E425C PDZ-peptide–stapled/open and 10% U-^{2}H, *proR* ILVM-$^{13}CH_3$ native protomers (so-called sample two above, Fig. 3*A* and *SI Appendix*, Fig. S4*A*, green), in the absence of added PDZ-peptide. Peak intensities in spectra recorded on the asymmetric sample derive primarily from configuration B [24.3/(24.3 + 2.7 × 2) × 100 = 82%; one unbound protomer

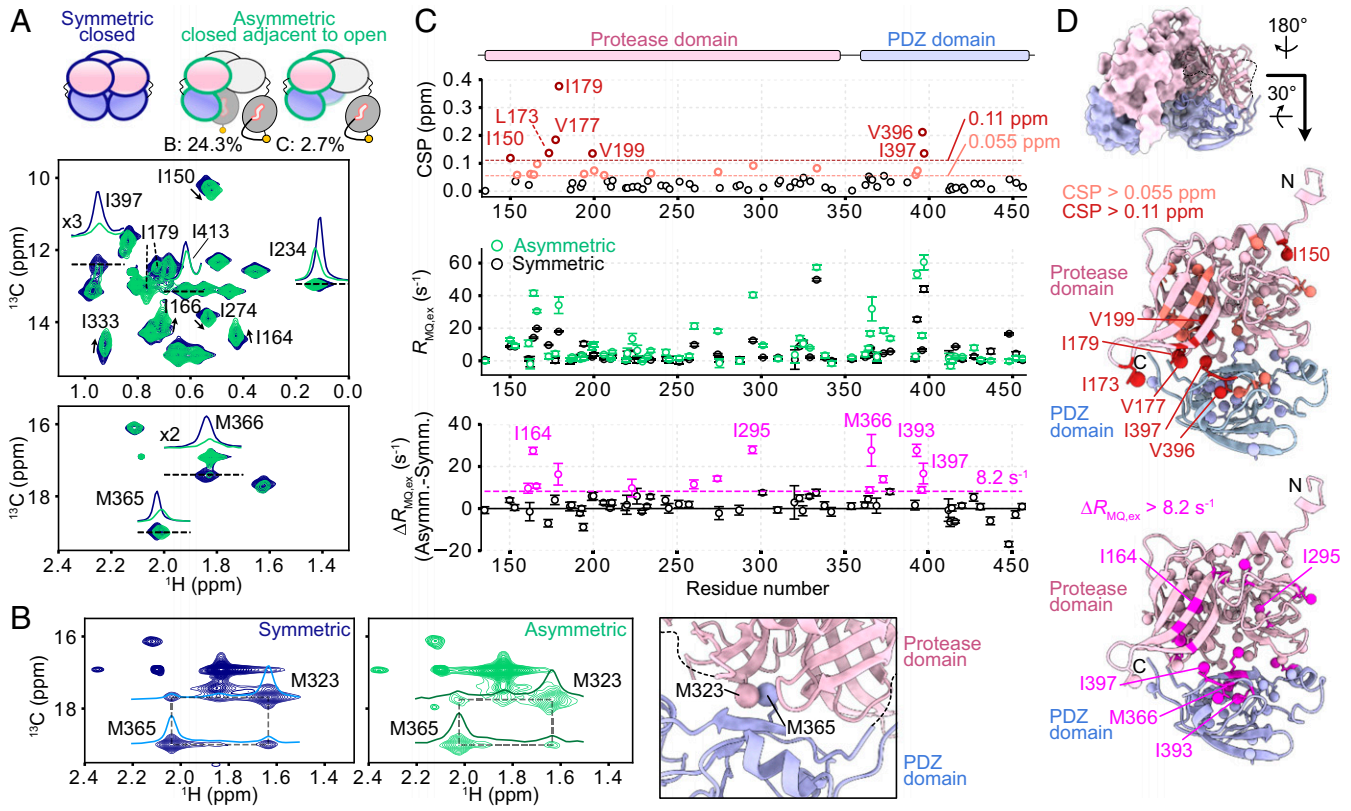

Fig. 3. Characterization of interprotomer allostery. (*A*) Superposition of ^{13}C-^{1}H HMQC spectra of the symmetric U-^{2}H, *proR* ILVM-$^{13}CH_3$ S306A/I441V HtrA2 sample (navy) and the asymmetric HtrA2 sample prepared by mixing 90% U-^{2}H, S306A/I441V/E425C PDZ-peptide–stapled/open protomers and 10% U-^{2}H, *proR* ILVM-$^{13}CH_3$ S306A/I441V protomers (green), focusing on the Ile (*Top*) and Met (*Bottom*) regions. The schematics for each sample are shown above the spectra. ^{1}H one-dimensional slices at the chemical shifts of the dotted lines are shown for I234, M365, M366, I397, and I413 in the same color as the two-dimensional contour. The slices for M366 and I397 are multiplied by factors of 2 and 3, respectively, for visualization. Methyl group assignments of the NMR closed protomer(s) of the asymmetric samples (green spectrum) were readily obtained from the assigned spectrum of the symmetric closed structure, as the chemical shift differences between the two spectra were small (<0.4 ppm, see *C*). The NMR datasets were recorded at 23.5 Tesla and 40 °C. (*B*) Selected regions of ^{1}H-^{13}C[t_1]-t_{mix}-^{1}H[t_2] NOESY spectra of the symmetric (*Left*) and asymmetric (*Right*) samples are shown (200 ms mixing time). Cross- and diagonal-peaks for M323 and M365 are connected with dotted boxes to aid in visualization. (*Right Inset*) A portion of the HtrA2 protomer structure (PDB ID: 1LCY) is shown, with the Cε carbons of M323 and M365 denoted as spheres. NMR datasets were recorded at 14.0 Tesla and 40 °C. (*C*, *Top*) Plot of CSP values between symmetric and asymmetric samples, 23.5 Tesla 40 °C. Methyl groups with CSPs larger than one (light orange) or two (dark red) SD (>0.055 and 0.11 ppm, respectively) are indicated. CSP values for each type of methyl-bearing residue were calculated as $\Delta\delta = \sqrt{(\Delta\delta_H/\alpha)^2 + (\Delta\delta_C/\beta)^2}$, where $\Delta\delta_H$ and $\Delta\delta_C$ are the chemical shift differences in the ^{1}H and ^{13}C dimensions, and α and β are the SDs of the ^{1}H and ^{13}C chemical shift distributions deposited in the Biological Magnetic Resonance Data Bank ($\alpha = 0.282$, $\beta = 1.646$ for Ile; $\alpha = 0.273$, $\beta = 1.582$ for Leu; $\alpha = 0.259$, $\beta = 1.358$ for Val; $\alpha = 0.387$, $\beta = 1.736$ for Met). (*Middle*) Plot of the exchange contributions to ^{13}C-^{1}H MQ relaxation rates ($R_{MQ,ex}$) for the symmetric (black circle) and asymmetric (green circle) HtrA2 samples at 14.0 Tesla. (*Bottom*) Plot of the difference in $R_{MQ,ex}$ values between symmetric and asymmetric samples ($\Delta R_{MQ,ex}$) calculated as $\Delta R_{MQ,ex} = R_{MQ,ex}$[asymmetric] − $R_{MQ,ex}$[symmetric]. $\Delta R_{MQ,ex}$ values larger than one SD (>8.2 s^{-1}) are colored in magenta, and those larger than two SD (>16.4 s^{-1}) are labeled by methyl residue. (*D*) *proR* ILVM-methyl groups from *C* with significant CSPs (>1 SD) (*Top*, light orange and deep red spheres) and $\Delta R_{MQ,ex}$ values (*Bottom*, magenta spheres) mapped onto the HtrA2 protomer (PDB ID: 1LCY). Effective concentrations of NMR-active protomers in particles B and C were 20 and 4.5 μM, respectively.

and two open/PDZ-peptide–stapled protomers; Fig. 3*A*], with the remaining contribution from HtrA2 molecules with two unbound protomers and a single open/PDZ-peptide–containing subunit [configuration C; $(2.7 \times 2)/(24.3 + 2.7 \times 2) \times 100 = 18\%$). Note that only unbound protomers are NMR active. As only small CSPs are observed, the unbound protomers in the asymmetric sample are in a closed position with the interface between protease and PDZ domains preserved as expected (Fig. 1*A*), which is further confirmed through the measurement of two-dimensional ^{13}C-edited NOESY spectra (^{1}H-^{13}C[t_1]-t_{mix}-^{1}H[t_2], where t_i is an acquisition time and t_{mix} the mixing time) in which an interdomain NOE connecting M323 from the protease domain and M365 from the PDZ domain is clearly observed (Fig. 3*B*).

Although the observed CSPs are small, they likely reflect subtle changes in the conformation of the unbound protomer caused by interprotomer allosteric effects that extend from the peptide-bound, open subunits. Methyl groups with significant CSPs (sample two) were mapped onto the HtrA2 crystal structure, localizing to the interprotomer trimer interface on the protease domain as well as to the intraprotomer domain interface between the protease and the PDZ domains (Fig. 3 *C* and *D*, *Top* and *Middle*). Notably, in a control experiment involving a related asymmetric sample in which either one (18% signal intensity) or two protomers (82% signal) are S-S–locked/closed and prepared by mixing 90% U-^{2}H, M-^{13}CH$_3$ V226C/Y428C S-S–locked protomers and 10% U-^{2}H, *proR* ILV-^{13}CH$_3$ native protomers (so-called sample one), the spectrum was nearly superimposable with a dataset recorded on a symmetric closed sample (*SI Appendix*, Fig. S4 *B* and *C*). Thus, CSPs are not a priori observed between spectra recorded of asymmetric and symmetric HtrA2 samples (i.e., CSPs are not due to the Cys mutations in adjacent protomers in and of themselves) but, when present, inform on (often subtle) structural changes.

In addition to CSPs, significant reductions in cross-peak intensities were also observed in spectra recorded of the asymmetric sample (sample two) due to signal broadening, indicating increases in μs–ms timescale conformational dynamics. This is readily apparent when one-dimensional traces along the ^{1}H dimension are highlighted (Fig. 3*A*). We quantified the exchange-induced broadening effects ($R_{MQ,ex}$) by measuring the difference in ^{13}C-^{1}H multiple-quantum (MQ) relaxation rates obtained with two different Carr–Purcell–Meiboom–Gill (CPMG) fields (66 and 2,000 Hz) (*SI Appendix*, Fig. S5) (49). The differences in per-residue $R_{MQ,ex}$ rates between asymmetric (sample two, shown schematically in Fig. 3*A*) and symmetric samples ($\Delta R_{MQ,ex} = R_{MQ,ex}$ [asymmetric] − $R_{MQ,ex}$ [symmetric]) were calculated, and residues with significant $\Delta R_{MQ,ex}$ rates were mapped onto the HtrA2 structure (Fig. 3 *C*, *Middle* and *Bottom* and *D*, *Bottom*). Notably, similar sets of methyl groups showed significant $\Delta R_{MQ,ex}$ values and CSPs (compare Fig. 3 *D*, *Center* and *Bottom*). We observed only one methyl group (L448δ1 within the PDZ domain) with a large negative $\Delta R_{MQ,ex}$ value, likely reflecting a weak trimer–hexamer exchange process for the symmetric sample, as L448δ1 has the largest chemical shift change between trimer and hexamer structures and is localized to the hexamerization interface (26). This exchange contribution is efficiently suppressed in the asymmetric sample, presumably because the apo hexameric structure cannot be formed from asymmetric trimers, in agreement with our structural model of the apo HtrA2 hexamer (26). The MQ relaxation rates recorded at high CPMG pulsing values (2 kHz) contain only minimal contributions from the exchange between states with lifetimes greater than ~500 μs. In the absence of exchange, or when contributions are minimal, these rates can be used to provide estimates of ps–ns timescale dynamics (49). Marked differences between rates measured for the symmetric (29.3 ± 12.5 s^{-1}, average ± SD) and asymmetric (32.6 ± 15.7 s^{-1}, average ± SD) samples were not observed, and the per-residue distributions were quite uniform in both cases, indicating that changes to faster timescale dynamics are likely not exploited by HtrA2 for intersubunit communication (*SI Appendix*, Fig. S5).

These results provide some insight into the interprotomer allosteric pathway. For example, as interprotomer PDZ–PDZ interactions are not observed in the crystal structure of HtrA2, it is reasonable to assume that the small but significant CSPs and $\Delta R_{MQ,ex}$ values noted for residues at the protease–protease domain interface within the asymmetric trimer highlight subtle changes in protease domain structure and in dynamics that reflect interprotomer communication. Our data suggest that the neighboring open, PDZ-peptide–bound subunits perturb the structural dynamics of the unbound, closed protomer so that its protease-PDZ interface becomes structurally heterogeneous. As the PDZ-peptide–binding site is located at this domain interface (21, 22), the structural heterogeneity may well underly the enhanced binding affinity for the PDZ-peptide, potentially signaling a weakening of this interface, when the neighboring subunits are already peptide bound.

The Symmetric, Fully Peptide-Bound Open State Is Required for HtrA2 Catalytic Activity. Having shown that interprotomer interactions regulate the binding affinity of the PDZ-peptide, we next sought to examine further how intersubunit allostery might modulate catalysis. To this end, we prepared mixed trimers and measured their peptidase activities to establish how the catalytic activity of an open/PDZ-peptide–bound protomer is affected by the conformational states of its neighbors. A set of samples was generated in which wild-type protomers harboring the catalytically active S306 residue (Fig. 4*A*, white circles) were mixed in different molar ratios with catalytically inactive S306A protomers containing the V226C/Y428C mutations for S-S locking of the PDZ domains (Fig. 4*A*, black-filled circles). The resultant mixture contains four unique trimers with different protomeric compositions, including configuration A comprising three S-S–locked protomers, configuration B composed of two S-S–locked protomers and one wild-type protomer, configuration C containing one S-S–locked protomer and two wild-type protomers, and configuration D with three wild-type protomers. Defining the fraction of wild-type subunits that are mixed as x, and assuming that protomers mix randomly (*SI Appendix*, Fig. S2), particles A to D are produced with molar ratios of $(1-x)^3$, $3x(1-x)^2$, $3x^2(1-x)$, and x^3, respectively (Fig. 4*A*).

Peptidase activities of mixed samples prepared with x ranging from 0 to 1 were measured under oxidizing conditions and in the presence of 1 mM PDZ-peptide (100 nM in subunit HtrA2 concentration). In this setup, the V226C/Y428C/S306A protomers are S-S–locked/closed and hence PDZ-peptide–binding incompetent, while the wild-type protomers are expected to form the open/PDZ-peptide–bound conformation. Interestingly, the peptidase activity did not follow a $y = x$ relationship, where y is the normalized activity, that would be expected from a simple model in which all of the wild-type protomers in configurations B to D are equally active (Fig. 4*B* and Model 1 in *SI Appendix*, Fig. S6). Instead, the activity profile clearly followed a $y = x^3$ relationship so that configuration D with three wild-type protomers is the only catalytically active state of HtrA2 (Fig. 4*B* and Model 3 in *SI Appendix*, Fig. S6). The activity profile could not be fit to other models, such as one assuming that the wild-type protomers in configurations C and D are catalytically active (Model 2 in *SI Appendix*, Fig. S6). As a control, we conducted the same assays in the presence of a reducing agent in which the disulfide bond connecting positions 226 and 428 is reduced so that all protomers in each particle would form open/PDZ-peptide–bound conformations upon the addition of excess PDZ-peptide. The activity profile now followed a $y = x$ relationship. Thus, the observed $y = x^3$ relationship under oxidizing conditions results from the closed conformational state of the PDZ domains in the V226C/Y428C/S306A S-S–locked protomers and the fact that they can, therefore, not bind peptide. Only when neighboring subunits are peptide-loaded, and hence in the open state, can the adjacent protomers become catalytically active. Our data highlight that there is a tight layer of interprotomer communication that allows only the fully bound symmetric form of HtrA2 to cleave substrate and,

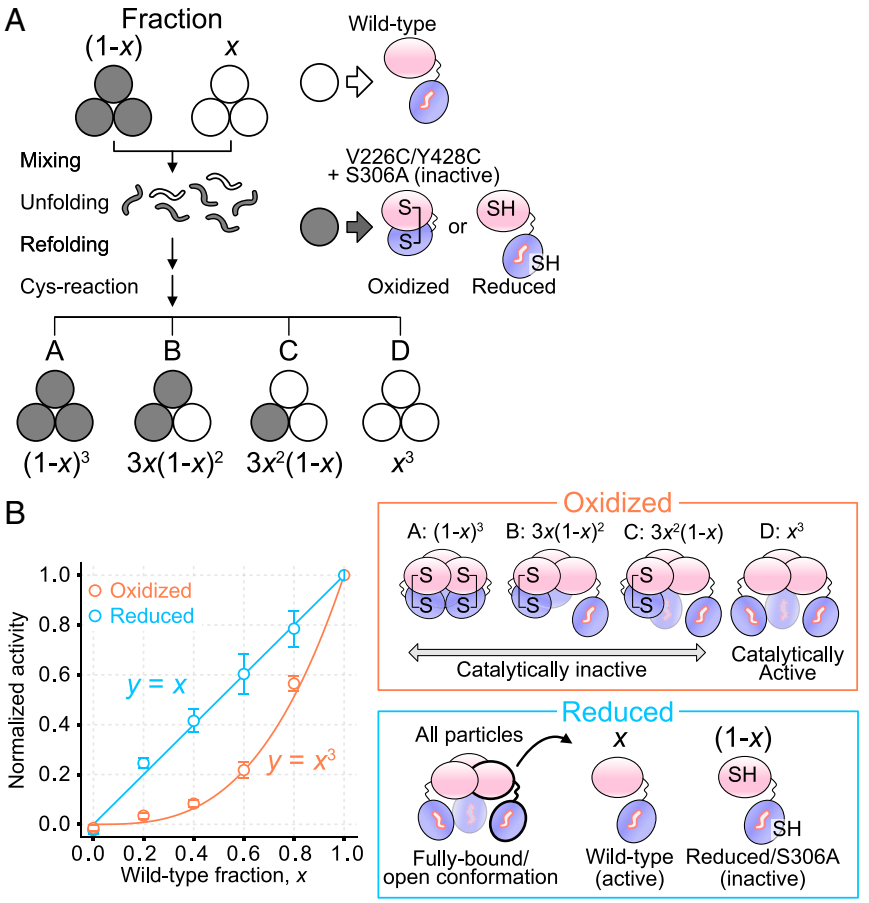

Fig. 4. Only the fully PDZ-peptide–bound state of HtrA2 is catalytically active. (*A*) Schematic of the procedure used to prepare mixed HtrA2 trimers for peptidase assays. HtrA2 trimers are shown as three circles. Wild-type protomers are denoted by white circles, and V226C/Y428C/S306A protomers are shown as gray-filled circles. Wild-type and V226C/Y428C/S306A protomers were mixed in the ratio of x:$(1 - x)$. Particles A to D of HtrA2 trimers are shown, along with their expected fractional populations assuming random mixing. Only one out of the three possible rotationally equivalent configurations is shown for particles B and C. (*B*) Plots of normalized peptidase activities (*Left*) under oxidizing (orange circle) and reducing (blue circle) conditions as a function of the molar fraction of wild-type protomers. Error bars correspond to one SD based on triplicate measurements. The curves corresponding to models of HtrA2 activity assuming that only the fully open, peptide-bound state is active ($y = x^3$, orange) or where all peptide-bound forms of HtrA2 are active ($y = x$, blue) are shown. Schematics of the four different species present under oxidizing conditions (*Right, Top*) and of a fully bound/open form under reducing conditions, where the probabilities of wild-type and S306A(V226C/Y428C) protomers are x and $(1 - x)$, respectively, as indicated (*Right, Bottom*). Note that excess PDZ-peptide has been added to ensure that any protomer that is not disulfide linked is in the open state. Absolute activities of oxidized and reduced states for $x = 1$ were within experimental error.

furthermore, that the allostery between HtrA2 protomers is not communicated at the level of active sites but, rather, is controlled via the open/closed status of the PDZ domains.

Catalysis Requires Structural Rearrangements That Can Only Occur in the Symmetric Open Conformation. In order to address the question of why only the fully bound, open conformation of HtrA2 can become catalytically active, we start by an NMR analysis of substrate peptide binding to the protease domains of symmetric and asymmetric HtrA2 trimers prepared using our protomer mixing protocol. We used an 11-residue substrate peptide (IRRVSYSFKKK), which has the same amino acid sequence as the fluorescent peptide that was used in the peptidase assays described above but lacks the fluorophore and quencher groups (25, 26). The binding of this substrate peptide to the symmetric native protein did not occur in the absence of the PDZ-peptide as expected since the substrate peptide-binding site is sequestered in the closed protomer conformation (*SI Appendix*, Fig. S7*A*). However, upon the binding of substrate in the presence of 1 mM PDZ-peptide, large chemical shifts were observed, and an apparent association constant of ~4,000 M^{-1} could be calculated from an analysis of the titration series (Fig. 5 *A*, *Left* and *Center* and *SI Appendix*, Fig. S7*B* and *Materials and Methods*). Notably, we observed large chemical shift differences for methyl groups on the protease domain (I150 and I274) located at the interprotomer interface and for I229 that is adjacent to a residue forming the catalytic center (D228), while CSPs were not observed for the methyl groups from the PDZ domain (Fig. 5*B*). These spectral changes suggest that substrate binding leads to structural rearrangements involving interprotease domain contacts and catalytic residues and, hence, to a structure that is distinct from the open/PDZ-peptide–bound but substrate-unbound conformation (and referred to subsequently as the "active" conformation). As with the binding of the PDZ-peptide, the low substrate affinity and separate resonances for some of the peaks corresponding to substrate-bound and free states argues that the subunit conformational change is much slower than initial substrate engagement. Interestingly, we note that a very weak NMR signal from I150 reporting on the active state was observed in the absence of substrate, which we attribute to the binding of the PDZ-peptide to the protease domain active site at high PDZ-peptide concentrations (*SI Appendix*, Fig. S7 *B* and *C*). As described in some detail in *SI Appendix*, *SI Text*, under the conditions of the

substrate titration (200 mM NaCl, 40 °C), HtrA2 is largely in a hexameric state as opposed to a trimer at low salt concentrations. The only very small CSPs upon hexamerization from the trimer are consistent with little change in subunit structure between the trimeric and hexameric forms of the enzyme, so that the structural changes noted for the hexamer upon substrate binding from the titration would be expected to also occur for HtrA2 in the trimeric state at lower concentrations (see *SI Appendix* for further discussion).

Since the formation of the active conformation upon substrate binding is accompanied by significant interprotomer structural rearrangements and, furthermore, since only when all three protomers are in the open conformation can activity occur, we reasoned that the transformation from an open state to a substrate-engaged active conformation likely involves a highly cooperative transition. If this is the case, then substrate binding at one protomer would be strongly modulated by the open/closed status of its neighbors, explaining why only the P_3L_3 state can become activated. To test this hypothesis, we analyzed the binding of substrate to an asymmetric HtrA2 sample prepared by mixing 90% U-^{2}H, M-$^{13}CH_3$ V226C/Y428C S-S–locked/closed and 10% U-^{2}H, *proR* ILV-$^{13}CH_3$ native protomers in the presence of 1 mM PDZ-peptide (Fig. 5 *A*, *Right* and *SI Appendix*, Fig. S7*D*), where the NMR signal derives only from protomers that are in the open state and surrounded by locked neighbors. Notably, the spectrum did not change upon the addition of a large excess of substrate (2 mM) so that the formation of the active conformation was effectively suppressed in the asymmetric sample. This clearly demonstrates that the active HtrA2 conformation can only be formed from the symmetric open conformation in which all PDZ domains are PDZ-peptide bound, consistent with results from the peptidase assays.

Disruption of the Interprotomer HtrA2 Allosteric Network Underlies Loss of Function in the S276C Disease Mutant. Our results demonstrate that HtrA2 function is tightly regulated through an intersubunit allosteric signaling network that spans the trimeric structure of the enzyme. We therefore wondered whether dysregulation of

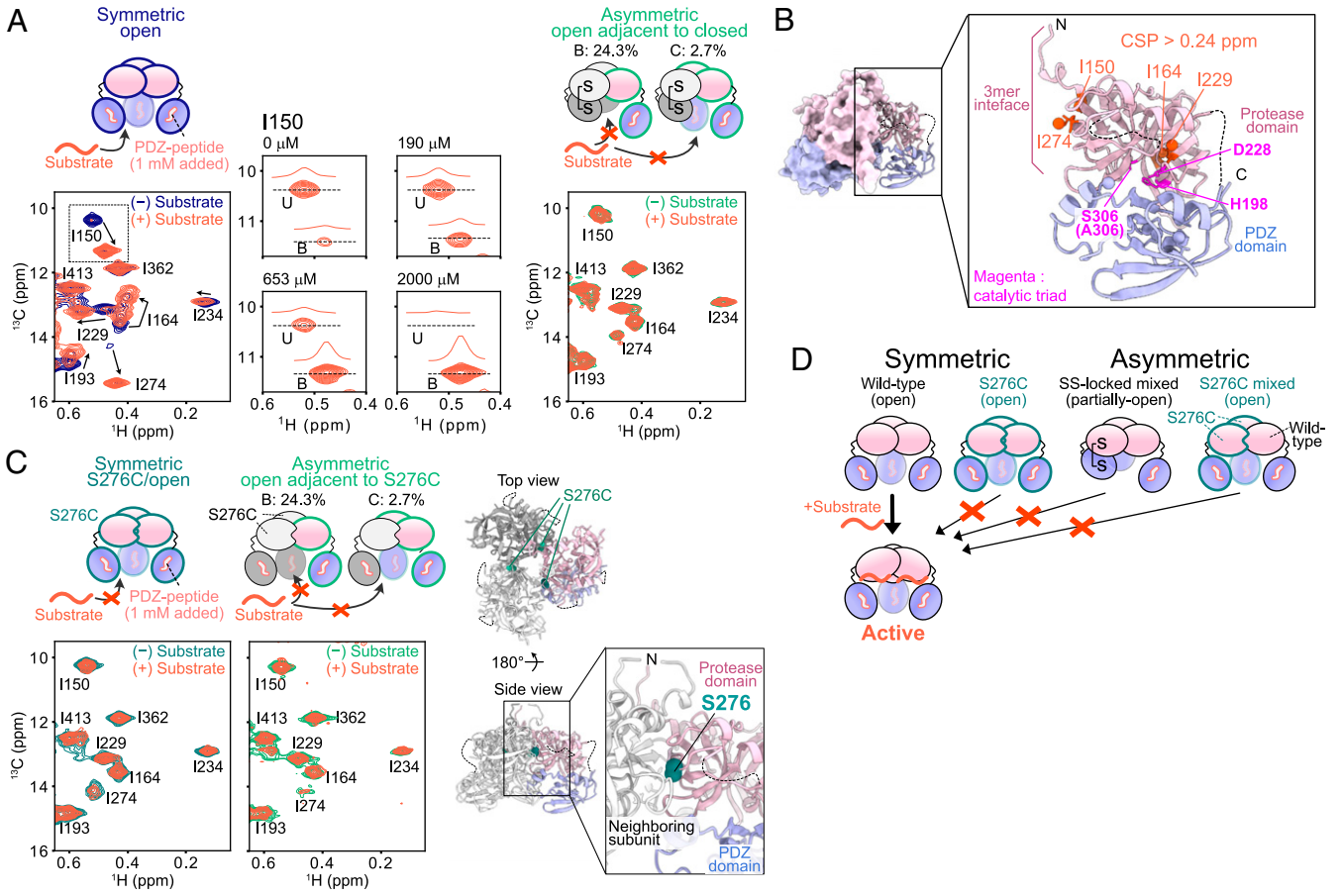

Fig. 5. Interprotomer allostery regulates formation of the active conformation. (*A*, *Left*) Superposition of ^{13}C-^{1}H HMQC spectra of the symmetric U-^{2}H, *proR* ILVM-$^{13}CH_3$ S306A/I441V HtrA2 sample (100 μM), 1 mM PDZ-peptide, in the absence (navy) and presence (orange) of 2 mM substrate (20-fold excess over HtrA2 protomers). (*Center*) Selected region of HMQC datasets recorded at four different concentrations of substrate (0, 190, 653, and 2,000 μM) and focusing on I150, located at the interprotomer domain interface (see *B*). (*Right*) Superposition of ^{13}C-^{1}H HMQC spectra of the asymmetric HtrA2 sample (150 μM), prepared by mixing 90% U-^{2}H, Met-$^{13}CH_3$ V226C/Y428C/S306A/I441V S-S–locked/closed protomers and 10% U-^{2}H, *proR* ILV-$^{13}CH_3$ S306A/I441V protomers, 1 mM PDZ-peptide, in the absence (light green) and presence (orange) of 2 mM substrate. The schematics for each type of sample are shown on top of the spectra. (*B*) Ile methyl groups with significant CSPs (>1 SD = 0.24 ppm) upon substrate binding are mapped onto an HtrA2 protomer (PDB ID: 1LCY) in orange, with remaining Ile methyl carbons highlighted as spheres. The residues forming the catalytic triad, H198, D228, and S306 (Ala in the structure), are shown as magenta sticks. CSPs were calculated as described in the legend to Fig. 3*C*. (*C*, *Left*) Superposition of ^{13}C-^{1}H HMQC spectra of the symmetric U-^{2}H, ILVM-$^{13}CH_3$ S276C/S306A/I441V HtrA2 sample in the absence (deep green) and presence (orange) of 2 mM substrate. (*Right*) Superposition of ^{13}C-^{1}H HMQC spectra of the asymmetric HtrA2 sample prepared by mixing 90% U-^{2}H, S276C/S306A/I441V protomers and 10% U-^{2}H, *proR* ILVM-$^{13}CH_3$ S306A/I441V protomers in the absence (light green) and presence (orange) of 2 mM substrate. Schematics for each type of sample are shown above the spectra. (*Right Inset*) S276 atoms are shown as spheres in the HtrA2 trimer structure (PDB ID: 1LCY). The neighboring subunit is colored in gray for visualization. (*D*) Schematic summarizing the NMR experiments shown in *A* and *C*. All NMR data sets were recorded at 23.5 Tesla and 40 °C in the presence of 200 mM NaCl.

this pathway might be at the root cause for loss of function of the S276C disease mutant, which was originally identified in *mnd2* mice, an animal model for Parkinson's disease (20). Although the S276C mutation abolishes the catalytic activity of HtrA2, it is located far from the substrate-binding/active site [the distance between S276 Cα and the nearest catalytic triad residue S306 Cα is >18 Å in the crystal structure (21)], residing within the interprotomer interface (Fig. 5 *C*, *Right*). Thus, it is reasonable to hypothesize that the S276C substitution may play a role in modulating communication between subunits.

In order to explore the underlying mechanism responsible for the loss of function of the S276C mutant, we first prepared a symmetric sample of S276C HtrA2 with U-^{2}H, ILVM-$^{13}CH_3$ labeling and recorded HMQC spectra with and without the PDZ-peptide. NMR spectra of the apo and PDZ-peptide bound states overlaid well with the corresponding spectra for HtrA2 without the S276C mutation. Small CSPs were only observed for some of the methyl groups proximal to S276, confirming that the overall structural differences in the S276C mutant are minimal and that S276C HtrA2 retains its ability to bind to the PDZ-peptide, consistent with expectations based on the crystal structure of this mutant (27) (*SI Appendix*, Fig. S8 *A* and *B*). We also confirmed by SDS-PAGE that interprotomer disulfide bonds are not formed as a result of the mutation, which would lead to cross-linked dimers of HtrA2 (*SI Appendix*, Fig. S8*C*). Subsequently, HMQC spectra were recorded on symmetric S276C HtrA2 samples with and without 2 mM substrate in the presence of 1 mM PDZ-peptide to ensure the formation of fully open/PDZ-peptide–bound subunits (Fig. 5 *C*, *Left*). Notably, spectral changes were not observed upon the addition of 2 mM substrate, demonstrating that the S276C mutant is incapable of forming the active conformation.

In order to obtain further evidence that the S276C mutation disrupts an allosteric pathway that is essential for the rearrangement to the active state, we prepared an asymmetric HtrA2 sample by mixing 90% U-^{2}H S276C mutant protomers (NMR invisible) and 10% U-^{2}H, *proR* ILVM-$^{13}CH_3$ native protomers (NMR visible) in the presence of 1 mM PDZ-peptide (Fig. 5 *C*, *Right*). Particles with either one or two native subunits could be observed in NMR spectra, corresponding to 82 and 18% of the resulting signal, respectively, and hence, the effect of neighboring S276C protomers on substrate binding to wild-type protomers could be established. Interestingly, even in the presence of >~30-fold excess substrate (2 mM) over HtrA2-binding sites, the active conformation was not observed. Clearly, the presence of at least one diseased protomer is able to disrupt the ability of the remaining native subunits to transition from the PDZ-bound/open conformation to the active state, as noted for the case of asymmetric molecules comprising mixtures of native and disulfide-locked subunits. The structural transition to an active conformation is thus a highly concerted process involving all three wild-type protomers in a trimer communicating via an intact allosteric signaling network (Fig. 5*D*).

Discussion

In this study, we have elucidated the important role of interprotomer communication in regulating the function of the HtrA2 chaperone/protease that plays an integral role in mitochondrial proteostasis (13–17). This was achieved by preparing HtrA2 subunits in defined conformational states through Cys-based chemistry followed by using a subunit mixing strategy to generate symmetric and asymmetric HtrA2 molecules that could then be studied by methyl-TROSY–based NMR spectroscopy. In this study and in the one preceding it by our group (26), we have chosen to work with peptides that either bind to PDZ domains or to the catalytic (substrate-binding) sites so as to separate these two binding processes and establish how each affects the structural dynamics of HtrA2. Physiological protein substrates would normally bind to the PDZ domain via C-terminal residues and to the active site via a two-pronged mechanism.

Our results establish that HtrA2 function is regulated on several different levels (Fig. 6). First, we previously showed that trimeric apo-HtrA2 dimerizes to form a hexameric structure, which has a much lower affinity for the PDZ-peptide, hence serving as a reservoir for HtrA2 trimers (26). Second, the binding of the PDZ-peptide (or the C terminus of HtrA2 substrates) to PDZ domains of HtrA2 occurs in a positive cooperative sequential process, forming an open conformation that is not yet active. The binding of the PDZ-peptide to one subunit allosterically primes adjacent subunits for subsequent binding. Third, the active conformation is generated in a highly cooperative, concerted manner through an interprotomer allosteric network.

A picture emerges whereby the binding of a PDZ-peptide is transmitted to adjacent protomers through interprotomer protease–protease domain interfaces. This leads to changes in structural dynamics in the neighboring (unbound) protomers, specifically at the intrasubunit protease-PDZ domain interface that is captured in our experiments as increases in μs–ms timescale conformational exchange. The altered dynamics at the domain interface likely "prime" the PDZ domain to open, hence underlying the positive cooperative binding of successive peptides. The open/PDZ-peptide–bound HtrA2 conformation (all three subunits are bound) is not yet catalytically active (i.e., it is open inactive). An active state occurs through the binding of substrate that is accompanied by a concerted conformational transition requiring the participation of all three subunits of the trimer. When one (or more) of the protomers is fixed in a closed conformation, or contains the S276C disease mutation, an active state cannot be formed. It is likely that this extensive interprotomer allosteric regulation is important for the function of HtrA2 as a stress-protective protease. The activation scheme described above ensures that HtrA2 is maintained in an inactive conformation until all three PDZ domains are occupied with PDZ-binding motifs from substrates. Thus, HtrA2 becomes catalytically active only when the concentration of potential substrates is high and therefore toxic to the cell, and uncontrolled cleavage of nonsubstrate proteins under basal conditions is thus suppressed.

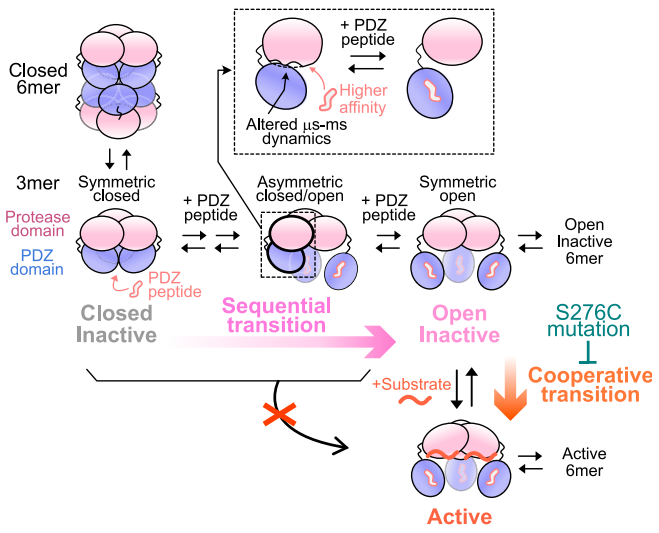

Fig. 6. Summary of the interprotomer allosteric regulation of HtrA2 activation. HtrA2 oligomerization in the apo state, sequential PDZ-peptide binding to HtrA2, and the formation of the active conformation of HtrA2 upon the binding of substrate are summarized in schematic form. The S276C mutation inhibits the formation of the active conformation of HtrA2.

The functional importance of the HtrA2 trimeric architecture is made clear in the context of the intersubunit allosteric network identified in this work. Indeed, monomeric mutants of HtrA2 are known to be inactive (21, 28, 29), suggesting that closed to open/active structural rearrangements require an oligomeric background. Dysregulation of the allosteric network that couples subunits within the trimer through mutations at the protomer–protomer interface can lead to disease. For example, the S276C HtrA2 mutant is catalytically inactive, and our studies show that the concerted motions of the protease domains within HtrA2 can no longer occur. Heterozygous *mnd2* mice, having only one copy of the S276C mutant allele, do not exhibit early lethality, yet the HtrA2 extracted from these animals shows reduced activity (~50 to 70%) (20, 50, 51). In line with our HtrA2 activation scheme, the considerable dominant-negative effect of the mutant allele in heterozygous mice likely results because a major fraction of the assembled HtrA2 trimers contain one or more S276C mutant protomers and is therefore not functional. Partial HtrA2 activity would be observed, however, since a nonzero fraction of functional HtrA2 trimers (i.e., all three protomers are wild type) would be present. We note that the physiological consequences of having hetero-oligomeric particles containing one or more protomers with disease mutations have been studied for VCP/p97, a human proteostasis protein, using a similar NMR-based approach (41).

Our detailed structural description of the HtrA2 activation mechanism is of interest for understanding the function of oligomeric proteins within the framework of the classical models describing allostery. Our functional data establish that the sequential binding of PDZ-peptides to HtrA2 occurs with concomitant PDZ domain opening, consistent with the well-known Koshland–Némethy–Filmer (sequential) description of allosteric-binding transitions (52). On the other hand, we have shown that the subsequent open/inactive to active conformational reorganization of the protease domains is likely to be highly concerted. This type of structural transition is in line with the Monod–Wyman–Changeux (concerted) model of allostery (53). Notably, these two binding processes occur within different domains of the HtrA2 protomer, with very different sets of domain interactions at play. For example, interprotomer contacts are exclusively formed between protease domains, and interprotomer PDZ–PDZ interactions are not observed. It is therefore not surprising that the binding events can be described by opposing classical models of allostery or via what is often referred to as nested allostery (54–56).

We have demonstrated that HtrA2 function is tightly regulated through an extensive interprotomer allosteric network involving a homo-trimeric architecture. Central to this work has been the utility of solution NMR spectroscopy to focus on a single protomer in the context of an oligomeric structure, thus providing insights into allosteric processes that cannot be obtained through bulk studies in which all protomers contribute to the observed signal. The strategies developed here pave the way for further elucidation of the important ways in which interprotomer allostery regulates both function and misfunction in oligomeric proteins.

Materials and Methods

HtrA2 proteins were expressed in *Escherichia coli* and purified by Ni-affinity chromatography, hydrophobic interaction chromatography, and size exclusion chromatography. All NMR measurements were performed at 23.5 Tesla (1 GHz ^{1}H frequency) or 14.0 Tesla (600 MHz ^{1}H frequency). The structures of HtrA2 for visualization were generated using UCSF ChimeraX (57). Details of protein expression and purification and of NMR experiments are provided in *SI Appendix*.

Data Availability. All relevant data are included in the paper and *SI Appendix*.

ACKNOWLEDGMENTS. Y.T. is supported through a Japan Society for the Promotion of Science Overseas Research Fellowship and an Uehara Memorial Foundation postdoctoral fellowship. R.W.H. is grateful to the Canadian Institutes of Health Research (CIHR) for a postdoctoral fellowship. This research is funded through grants from the CIHR and the Natural Sciences and Engineering Research Council of Canada. L.E.K. holds a Canada Research Chair in Biochemistry. This study made use of NMRbox: National Center for Biomolecular NMR Data Processing and Analysis, a Biomedical Technology Research Resource, which is supported by NIH Grant P41GM111135 (National Institute of General Medical Sciences).

1. T. Clausen, M. Kaiser, R. Huber, M. Ehrmann, HTRA proteases: Regulated proteolysis in protein quality control. *Nat. Rev. Mol. Cell Biol.* **12**, 152–162 (2011).
2. D. Zurawa-Janicka *et al.*, Structural insights into the activation mechanisms of human HtrA serine proteases. *Arch. Biochem. Biophys.* **621**, 6–23 (2017).
3. L. Faccio *et al.*, Characterization of a novel human serine protease that has extensive homology to bacterial heat shock endoprotease HtrA and is regulated by kidney ischemia. *J. Biol. Chem.* **275**, 2581–2588 (2000).
4. C. W. Gray *et al.*, Characterization of human HtrA2, a novel serine protease involved in the mammalian cellular stress response. *Eur. J. Biochem.* **267**, 5699–5710 (2000).
5. Y. Suzuki *et al.*, A serine protease, HtrA2, is released from the mitochondria and interacts with XIAP, inducing cell death. *Mol. Cell* **8**, 613–621 (2001).
6. R. Hegde *et al.*, Identification of Omi/HtrA2 as a mitochondrial apoptotic serine protease that disrupts inhibitor of apoptosis protein-caspase interaction. *J. Biol. Chem.* **277**, 432–438 (2002).
7. A. M. Verhagen *et al.*, HtrA2 promotes cell death through its serine protease activity and its ability to antagonize inhibitor of apoptosis proteins. *J. Biol. Chem.* **277**, 445–454 (2002).
8. L. M. Martins *et al.*, The serine protease Omi/HtrA2 regulates apoptosis by binding XIAP through a reaper-like motif. *J. Biol. Chem.* **277**, 439–444 (2002).
9. G. van Loo *et al.*, The serine protease Omi/HtrA2 is released from mitochondria during apoptosis. Omi interacts with caspase-inhibitor XIAP and induces enhanced caspase activity. *Cell Death Differ.* **9**, 20–26 (2002).
10. S. M. Srinivasula *et al.*, Inhibitor of apoptosis proteins are substrates for the mitochondrial serine protease Omi/HtrA2. *J. Biol. Chem.* **278**, 31469–31472 (2003).
11. Q. H. Yang, R. Church-Hajduk, J. Ren, M. L. Newton, C. Du, Omi/HtrA2 catalytic cleavage of inhibitor of apoptosis (IAP) irreversibly inactivates IAPs and facilitates caspase activity in apoptosis. *Genes Dev.* **17**, 1487–1496 (2003).
12. Y. Suzuki, K. Takahashi-Niki, T. Akagi, T. Hashikawa, R. Takahashi, Mitochondrial protease Omi/HtrA2 enhances caspase activation through multiple pathways. *Cell Death Differ.* **11**, 208–216 (2004).
13. S. Radke *et al.*, Mitochondrial protein quality control by the proteasome involves ubiquitination and the protease Omi. *J. Biol. Chem.* **283**, 12681–12685 (2008).
14. N. Moisoi *et al.*, Mitochondrial dysfunction triggered by loss of HtrA2 results in the activation of a brain-specific transcriptional stress response. *Cell Death Differ.* **16**, 449–464 (2009).
15. L. M. Martins *et al.*, Neuroprotective role of the Reaper-related serine protease HtrA2/Omi revealed by targeted deletion in mice. *Mol. Cell. Biol.* **24**, 9848–9862 (2004).
16. H. Plun-Favreau *et al.*, The mitochondrial protease HtrA2 is regulated by Parkinson's disease-associated kinase PINK1. *Nat. Cell Biol.* **9**, 1243–1252 (2007).
17. E. Desideri, L. M. Martins, Mitochondrial stress signalling: HTRA2 and Parkinson's disease. *Int. J. Cell Biol.* **2012**, 607929 (2012).
18. K. M. Strauss *et al.*, Loss of function mutations in the gene encoding Omi/HtrA2 in Parkinson's disease. *Hum. Mol. Genet.* **14**, 2099–2111 (2005).
19. H. Unal Gulsuner *et al.*, Mitochondrial serine protease HTRA2 p.G399S in a kindred with essential tremor and Parkinson disease. *Proc. Natl. Acad. Sci. U.S.A.* **111**, 18285–18290 (2014).
20. J. M. Jones *et al.*, Loss of Omi mitochondrial protease activity causes the neuromuscular disorder of mnd2 mutant mice. *Nature* **425**, 721–727 (2003).
21. W. Li *et al.*, Structural insights into the pro-apoptotic function of mitochondrial serine protease HtrA2/Omi. *Nat. Struct. Biol.* **9**, 436–441 (2002).
22. Y. Zhang, B. A. Appleton, P. Wu, C. Wiesmann, S. S. Sidhu, Structural and functional analysis of the ligand specificity of the HtrA2/Omi PDZ domain. *Protein Sci.* **16**, 1738–1750 (2007).
23. N. P. Walsh, B. M. Alba, B. Bose, C. A. Gross, R. T. Sauer, OMP peptide signals initiate the envelope-stress response by activating DegS protease via relief of inhibition mediated by its PDZ domain. *Cell* **113**, 61–71 (2003).
24. J. Chien, M. Campioni, V. Shridhar, A. Baldi, HtrA serine proteases as potential therapeutic targets in cancer. *Curr. Cancer Drug Targets* **9**, 451–468 (2009).
25. L. M. Martins *et al.*, Binding specificity and regulation of the serine protease and PDZ domains of HtrA2/Omi. *J. Biol. Chem.* **278**, 49417–49427 (2003).
26. Y. Toyama, R. W. Harkness, T. Y. T. Lee, J. T. Maynes, L. E. Kay, Oligomeric assembly regulating mitochondrial HtrA2 function as examined by methyl-TROSY NMR. *Proc. Natl. Acad. Sci. U.S.A.* **118**, e2025022118 (2021).
27. A. R. Wagh, K. Bose, Structural basis of inactivation of human counterpart of mouse motor neuron degeneration 2 mutant in serine protease HtrA2. *Biosci. Rep.* **38**, 1–12 (2018).
28. M. K. Nam *et al.*, The homotrimeric structure of HtrA2 is indispensable for executing its serine protease activity. *Exp. Mol. Med.* **38**, 36–43 (2006).
29. L. K. Chaganti, R. R. Kuppili, K. Bose, Intricate structural coordination and domain plasticity regulate activity of serine protease HtrA2. *FASEB J.* **27**, 3054–3066 (2013).

30. G. P. Lisi, J. P. Loria, Solution NMR spectroscopy for the study of enzyme allostery. *Chem. Rev.* **116**, 6323–6369 (2016).
31. E. Freire, A. Schön, A. Velazquez-Campoy, Isothermal titration calorimetry: General formalism using binding polynomials. *Methods Enzymol.* **455**, 127–155 (2009).
32. I. Bahar, C. Chennubhotla, D. Tobi, Intrinsic dynamics of enzymes in the unbound state and relation to allosteric regulation. *Curr. Opin. Struct. Biol.* **17**, 633–640 (2007).
33. S. R. Tzeng, C. G. Kalodimos, Protein dynamics and allostery: An NMR view. *Curr. Opin. Struct. Biol.* **21**, 62–67 (2011).
34. R. B. Berlow, H. J. Dyson, P. E. Wright, Expanding the paradigm: Intrinsically disordered proteins and allosteric regulation. *J. Mol. Biol.* **430**, 2309–2320 (2018).
35. S. Y. Stevens, S. Sanker, C. Kent, E. R. P. Zuiderweg, Delineation of the allosteric mechanism of a cytidylyltransferase exhibiting negative cooperativity. *Nat. Struct. Biol.* **8**, 947–952 (2001).
36. N. Popovych, S. Sun, R. H. Ebright, C. G. Kalodimos, Dynamically driven protein allostery. *Nat. Struct. Mol. Biol.* **13**, 831–838 (2006).
37. J. Carlsson, H. Drevin, R. Axén, Protein thiolation and reversible protein-protein conjugation. *N*-Succinimidyl 3-(2-pyridyldithio)propionate, a new heterobifunctional reagent. *Biochem. J.* **173**, 723–737 (1978).
38. D. Barthelme, J. Z. Chen, J. Grabenstatter, T. A. Baker, R. T. Sauer, Architecture and assembly of the archaeal Cdc48*20S proteasome. *Proc. Natl. Acad. Sci. U.S.A.* **111**, E1687–E1694 (2014).
39. R. Huang *et al*., Unfolding the mechanism of the AAA+ unfoldase VAT by a combined cryo-EM, solution NMR study. *Proc. Natl. Acad. Sci. U.S.A.* **113**, E4190–E4199 (2016).
40. A. K. Schuetz, L. E. Kay, A dynamic molecular basis for malfunction in disease mutants of p97/VCP. *eLife* **5**, 1–25 (2016).
41. R. Huang, Z. A. Ripstein, J. L. Rubinstein, L. E. Kay, Cooperative subunit dynamics modulate p97 function. *Proc. Natl. Acad. Sci. U.S.A.* **116**, 158–167 (2019).
42. V. Tugarinov, V. Kanelis, L. E. Kay, Isotope labeling strategies for the study of high-molecular-weight proteins by solution NMR spectroscopy. *Nat. Protoc.* **1**, 749–754 (2006).
43. I. Gelis *et al*., Structural basis for signal-sequence recognition by the translocase motor SecA as determined by NMR. *Cell* **131**, 756–769 (2007).
44. P. Gans *et al*., Stereospecific isotopic labeling of methyl groups for NMR spectroscopic studies of high-molecular-weight proteins. *Angew. Chem. Int. Ed. Engl.* **49**, 1958–1962 (2010).
45. V. Tugarinov, P. M. Hwang, J. E. Ollerenshaw, L. E. Kay, Cross-correlated relaxation enhanced ^{1}H-^{13}C NMR spectroscopy of methyl groups in very high molecular weight proteins and protein complexes. *J. Am. Chem. Soc.* **125**, 10420–10428 (2003).
46. B. T. Falk, P. J. Sapienza, A. L. Lee, Chemical shift imprint of intersubunit communication in a symmetric homodimer. *Proc. Natl. Acad. Sci. U.S.A.* **113**, 9533–9538 (2016).
47. R. Huang, F. Pérez, L. E. Kay, Probing the cooperativity of *Thermoplasma acidophilum* proteasome core particle gating by NMR spectroscopy. *Proc. Natl. Acad. Sci. U.S.A.* **114**, E9846–E9854 (2017).
48. C. A. Waudby, A. Ramos, L. D. Cabrita, J. Christodoulou, Two-dimensional NMR lineshape analysis. *Sci. Rep.* **6**, 24826 (2016).
49. D. M. Korzhnev, K. Kloiber, V. Kanelis, V. Tugarinov, L. E. Kay, Probing slow dynamics in high molecular weight proteins by methyl-TROSY NMR spectroscopy: Application to a 723-residue enzyme. *J. Am. Chem. Soc.* **126**, 3964–3973 (2004).
50. W. Hur *et al*., Serine protease HtrA2/Omi deficiency impairs mitochondrial homeostasis and promotes hepatic fibrogenesis via activation of hepatic stellate cells. *Cells* **8**, 1–20 (2019).
51. H. Zhou *et al*., Loss of high-temperature requirement protein A2 protease activity induces mitonuclear imbalance via differential regulation of mitochondrial biogenesis in sarcopenia. *IUBMB Life* **72**, 1659–1679 (2020).
52. D. E. Koshland Jr, G. Némethy, D. Filmer, Comparison of experimental binding data and theoretical models in proteins containing subunits. *Biochemistry* **5**, 365–385 (1966).
53. J. Monod, J. Wyman, J. P. Changeux, On the nature of allosteric transitions: A plausible model. *J. Mol. Biol.* **12**, 88–118 (1965).
54. S. J. Gill, C. H. Robert, M. Coletta, E. Di Cera, M. Brunori, Cooperative free energies for nested allosteric models as applied to human hemoglobin. *Biophys. J.* **50**, 747–752 (1986).
55. M. A. Daugherty *et al*., Identification of the intermediate allosteric species in human hemoglobin reveals a molecular code for cooperative switching. *Proc. Natl. Acad. Sci. U.S.A.* **88**, 1110–1114 (1991).
56. O. Yifrach, A. Horovitz, Nested cooperativity in the ATPase activity of the oligomeric chaperonin GroEL. *Biochemistry* **34**, 5303–5308 (1995).
57. E. F. Pettersen *et al*., UCSF ChimeraX: Structure visualization for researchers, educators, and developers. *Protein Sci.* **30**, 70–82 (2021).